Indian Journal of Fibre & Textile Research
Vol. 51, September 2026, pp. 411-422
DOI: 10.56042/ijftr.v51i3.18683

Silica aerogel-embedded thermal liner: fabrication, properties, and potential for extreme heat protective clothing

Tathagata Das[1,2,a], Apurba Das[2], R Alagirusamy[2]

[1]Department of Fashion Technology, Sona College of Technology, Junction Main Rd, Salem, Tamil Nadu 636005
[2]Department of Textile and Fibre Engineering, Indian Institute of Technology Delhi, New Delhi, India, 110016

Received 9 April 2025; revised received and accepted 21 May 2026

Silica aerogel was developed in situ aramid needle punched nonwoven thermal liner via sol-gel process followed by ambient pressure drying technique using tetraethoxysilane (TEOS) as a precursor. The thermal liner was augmented with silica aerogel at three different add-on percentages relative to the weight of the nonwoven fabric. This incorporation aimed to investigate the influence of the aerogel add-on percentage on the thermal protective performance of the tested thermal liner. The wet gel surface was modified through a silylation process, varying concentrations of silylating agent, trimethylchlorosilane (TMCS), in hexane. The characterization of the aerogel-embedded thermal liner samples encompassed evaluations of thickness, air permeability, thermal conductivity, thermal stability (measured by TGA), and examination through Fourier-transform infrared spectroscopy (FTIR) and Scanning Electron Microscopy. The heat transfer index (HTI_{24}) was measured for every sample under radiant and flame heat exposure. An investigation using Analysis of Variance was carried out to evaluate how the percentage of aerogel add-on and concentrations of silylating agent affect the HTI_{24} heat transfer index (HTI_{24}) of the aerogel-embedded thermal line. Aerogel embedded thermal liner, irrespective of aerogel add-on percentages and TMCS concentrations, provides higher protection under both radiant and flame exposure than non-aerogel nonwoven thermal liner. Both aerogel add-on percentage and TMCS concentration positively impact the HTI_{24} value for both radiant and flame heat exposure. Higher protection against radiant and flame heat exposure makes aerogel-embedded thermal liners more suitable for extreme heat-protective clothing.

Keywords: Silica aerogel, Sol-Gel method, Ambient pressure drying technique, Thermal protective performance, Heat transfer index (HTI_{24}), Fire fighter clothing

1 Introduction

Firefighters encounter various levels of heat and flame exposure while performing their duties, which can lead to fatal or non-fatal injuries to the individuals. Extreme heat protective clothing is used to protect firefighters from burn injuries. The main objective of the firefighter suit is to provide the wearer with some degree of protection from burn injuries that occur due to fire hazards. A Firefighter suit restricts the penetration of heat energy from the environment to the wearer's body through the clothing. The clothing material should have very low thermal conductivity to reduce the penetration of heat energy. Along with thermal protection, the comfort of the firefighters is also a critical factor in designing a firefighter suit. Firefighter suits should be lightweight to provide the wearer with a higher degree of comfort and mobility. Thus, selecting material with high thermal insulation and low density is crucial to designing a firefighter suit.

Aerogel is a substance composed of three-dimensional open networks formed by polymer molecules or coherent nanoparticles [1–4]. They exhibit unique porous properties, featuring high transparency in the visible light spectrum, extremely low thermal conductivity (approximately 0.01 $Wm^{-1}K^{-1}$), a shallow sound velocity (below 100 m/s), and an expansive surface area reaching up to 1600 m^2/g [2,35,6]. Aerogels are made by taking all the liquid out of a wet gel using either the supercritical or ambient pressure drying method. Typically, aerogels are made using the supercritical drying method. However, the use of costly alkoxide precursors and the risks associated with the supercritical drying process of gels impede the mass production of aerogel materials and restrict their widespread application across diverse domains [7–9]. As a result, ambient pressure drying is a new promising technology for making silica aerogels on a large scale.

Because of these qualities, aerogels are used in many areas of technology [7,10–12]. For example, they are used as effective materials in the structure of

[a]Corresponding author.
E-mail: tathagatadas55@gmail.com

heat-insulating materials, in acoustic impedance modules, radio-luminescent modules, as liquid propellants in rockets, and as catalyst supports [13–17]. Aerogel is a good material for heat-insulating clothing because it doesn't conduct heat well and is very light.

But aerogels do face some problems when it comes to being used. Aerogels have the problem of soaking up moisture from the air, being brittle, and being hard to work with. They also can't insulate complex shapes well[16,18,19] . For this reason, a fiber-reinforced aerogel fabric has been developed as a substitute, aiming to achieve insulation materials that are more flexible, drapable, and durable. Nonwoven fabric stands out as a suitable material for reinforcement in this context[20]. Lee et al. [21] fabricated composite blankets made of silica aerogel, which exhibited low densities of 0.13 g cm^{-3}, high silica aerogel contents of 79 %, and low thermal conductivities of 18.92 mW m^{-1} K^{-1} in contrast to polyethylene (PE) blankets. Li et al. [19,20] .utilized aramid fibers as a reinforcement for silica aerogels, showcasing enhanced elasticity, flexibility, and notably low thermal conductivity [22,23]. They achieved a significantly low thermal conductivity of 0.0277±0.0007 $W.m^{-1}$. K^{-1}. Chakraborty et al. found that aerogel-embedded nonwoven fabric exhibits higher protection from extreme heat compared to ordinary non-aerogel nonwoven fabric.

However, very few studies have investigated the thermal protection performance of silica aerogel-embedded nonwoven thermal liner, along with different aerogel add-on percentages and different process parameters. A limited number of research studies have explored the thermal shielding capabilities of silica aerogel-embedded thermal liner under radiant and flame heat exposure.

In this study, a three-layer needle-punched aramid nonwoven thermal liner is selected as Das et al.[24] found that three-layer thermal liner provides better protection compared to single layers thermal liner. Silica aerogel was synthesized in situ the middle layer of the three-layer thermal liner using ambient pressure drying technique. Subsequent to their preparation, the aerogel-fabric samples underwent comprehensive characterization, encompassing assessments of thickness, air permeability, thermal conductivity, the formation of organic and inorganic bonds, and an evaluation of their protective capabilities against radiant and flame heat fluxes.

2 Materials and Methods

2.1 Materials

This study employed a three-layer thermal liner with a total areal density of 200 g/m^2. This composite consisted of three needle-punched Nomex IIIA nonwoven fabric layers, each having an individual areal density of 66 g/m^2. The nonwoven fabric was prepared from 38 mm Nomex IIIA staple fiber with a linear density of 1.5 denier. Figure 1(a) depicts the schematic diagram of a three-layer thermal liner. Table 1 enumerates the physical and thermal properties of the test thermal liner. Silica aerogel was developed in situ the middle layer of the thermal liner. Three distinct add-on percentages (20 %, 40 %, and 60 %) were implemented, corresponding to the weight of the middle layer of the thermal liner. This approach was employed to investigate the influence of the aerogel add-on percentage on the thermal protective performance of the three-layer thermal liner embedded with aerogel. For the preparation of silica aerogel Tetraethoxysilane (TEOS), Oxalic acid, [$(COOH)_2$. $2H_2O$], Ammonium Fluoride (NH_4F), Methanol, Trimethyl chlorosilane (TMCS), Hexane, and double distilled water were used.

2.1.1 Nonwoven Fabrics preparation

The nonwoven fabrics were developed by two step process. In the first step, the Nomex IIIA fibers were carded by Trytex carding machine to prepare fiber webs of the required areal density. In the next step, the fiber webs were mechanically bound by DILO needle punch nonwoven machine to produce nonwoven fabrics. The needle penetration depth and punch density were 5 mm and 50 punches/cm^2 in the punching process.

2.1.2 Silica Aerogel Synthesis

Silica aerogel was synthesized by a five-stapes process:

Table 1 — Physical and thermal properties of the test thermal liner

Parameters	Values
Total areal density of the thermal liner (g/m^2)	200
Divided into number of layers	3
Thickness (mm)	3.26
Bulk density (kg/m^3)	61
Porosity (%)	95.5
Air permeability (cm^3/cm^2/s)	138.89
Thermal conductivity (W/m.K)	0.074
Radiative heat transfer index (HTI_{24})	25
Flame heat transfer index (HTI_{24})	53

(a) Gel preparation: The sol-gel process was employed to synthesize the silica aerogel. Initially, a silica source solution was subjected to hydrolysis with the addition of an acid catalyst to prepare the sol. Subsequently, the sol was condensed by introducing a base catalyst, resulting in the formation of a silica gel.
(b) Aging of the gel: The prepared silica gel was aged in its mother solution to strengthen the gel.
(c) Solvent exchange: After aging, the dispersion medium of the silica gel was exchanged with a solvent with lower surface tension to reduce the capillary force during evaporation of the pore liquid.
(d) Silylation: The purpose of the silylating agent is to make the surface of the silica gel hydrophobic and give it the ability to spring back after it has dried.
(e) Drying the gel: Drying is the last and most important step in making silica aerogel. This process uses ambient pressure drying to remove pore liquid from silica gel.

Future work can focus on evaluating the long-term durability and washability of the aerogel-embedded thermal liners to ensure retention of thermal performance under repeated laundering and mechanical stress.

Figure 1(b) demonstrates the silica aerogel synthesis process in situ thermal liner.

Sol-Gel Process:

Silica aerogel was synthesized by means of a sequential acid-base procedure, succeeded by drying under ambient pressure conditions. Initially, a sol was prepared by diluting TEOS tetraethyl orthosilicate (TEOS) precursor with ethanol. Subsequently, oxalic acid [$(COOH)_2$, 0.001 M] was introduced into the sol and stirred for one hour. After mixing, the sol was allowed to remain at room temperature for twelve hours to facilitate hydrolysis. NH_4F was then incrementally applied drop by drop to the sol, and the mixture was stirred for three minutes. The molar ratio of TEOS: EtOH: $(COOH)_2$: NH_4F was maintained constant at 1: 38: 3.73 x 10^{-5}: 0.023. Following this, the sol was poured onto nonwoven fabric, placed in a petri dish, and put at room temperature to enable the formation of the silica gel.

Silylation and ambient pressure drying

After the gel set, thepetri dish with nonwoven was filled with excess ethanol and wrapped in aluminium foil. Thenonwovenwas then left alone for an hour to age. After the ageing process, ethanol was taken out and hexene was added in a solvent exchange process at 50 degrees Celsius in a shaker set to 120 rpms. This

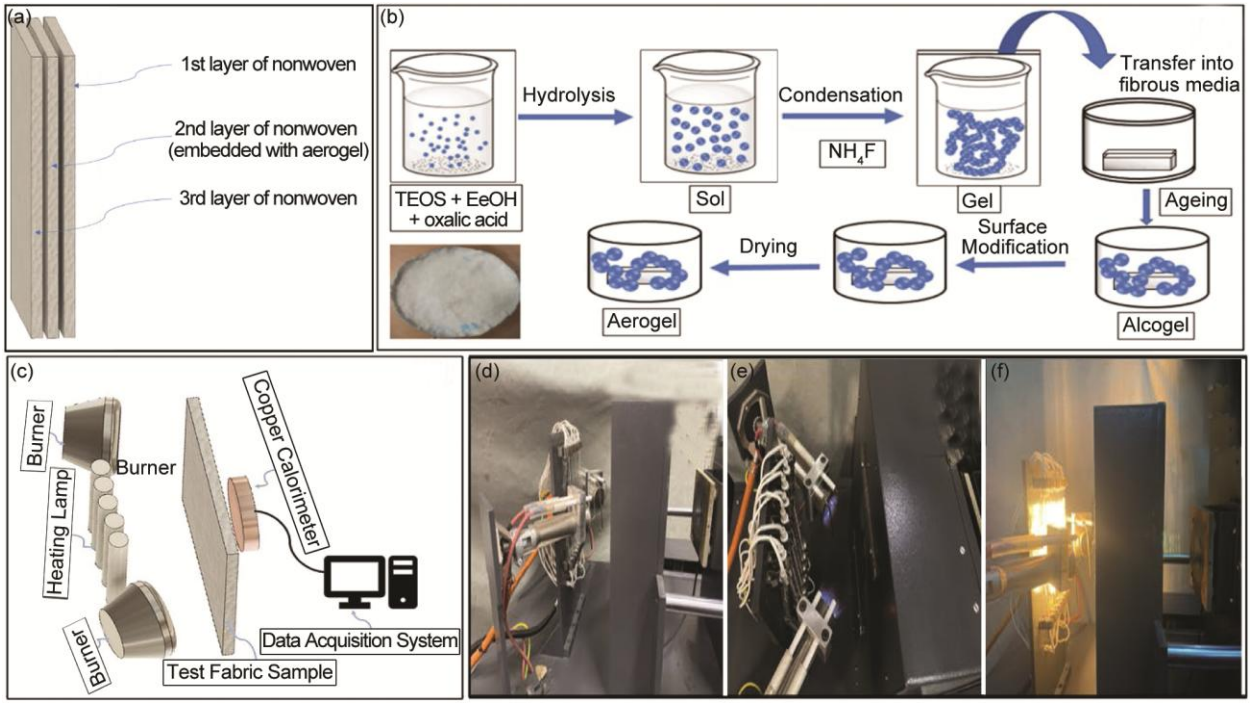

Figure 1 — (a) Schematic diagram of a three-layer thermal liner; (b) Silica aerogel synthesis process; (c) Schematic diagram of the thermal protective performance (TPP) tester; Testing instrument-(d) TPP tester,(e) Flame exposure, (f) Radiant exposure.

made it possible for the gel to completely change from ethanol to hexene. TMCS, a silylating agent, was added that makes things water-repellent and gives them a spring-back effect, and let it react with the gel for 16 hours in the same shaker, at the same temperature and speed as the solvent exchange reaction. Three levels of TMCS concentration (5%, 10%, and 15% TMCS) were utilized to see how the amount of the silylating agent changes the gel's properties. After silylation, any unreacted TMCS was exchanged with hexene, and the mixture was placed in a shaker for four hours at 50°C and 120 rpm. Subsequently, hexene was removed, and the silylated gel-embedded nonwoven fabric was dried for one hour at 50°C and then for an additional two hours at 100°C to obtain a hydrophobic aerogel-embedded composite nonwoven fabric.

TMCS concentration was varied to observe how it affects aerogel structural integrity and performance. TMCS replaces surface silanol (–Si–OH) groups with trimethylsilyl (–Si–$(CH_3)_3$) moieties. This reduces ambient pressure drying capillary strains and improves aerogel network hydrophobicity. Lower TMCS concentrations (5%), partial silylation may not be enough to reduce capillary-induced shrinking, resulting in enhanced densification and decreased pore preservation. Silanol substitution rises with TMCS concentration (10–15%), improving spring-back behaviour, structural collapse, and mesoporous architecture retention. If the silylating chemical concentration is too high, it may block pores, increase mass uptake, or unevenly cover the surface, affecting permeability and mechanical flexibility. To discover the optimal balance between hydrophobic modification, structural preservation, and aerogel performance, three TMCS concentrations were used.

2.2 Methods

2.2.1 Experimental Methods

To study the effect of aerogel on the protective performance of a three-layer thermal liner, three different add-on percentages (20 %, 40 %, and 60 %) were added on the basis of the weight of the middle layer of the thermal liner. Three different concentrations of silylating agent (5 %, 10 %, and 15 %) were used to analyze the effect of the silylating agent concentration on the synthesis of silica aerogel. Nine aerogel-embedded nonwoven samples were prepared with different add-on percentages and different concentrations of silylating agent. Table 2 shows the experimental plan.

Table 2 — Experimental plan

Samples	Add-on percentage (%)	Concentration of silylating agent (%)
1	20	5
2	20	10
3	20	15
4	40	5
5	40	10
6	40	15
7	60	5
8	60	10
9	60	15

2.2.2 Methods of Characterization:

Surface morphology:

The surface morphology of the developed silica aerogel was investigated using a scanning electron microscope (SEM), specifically a Zeiss EVO 18 model. The acceleration voltage was set at 20 kV. Prior to Analysis, the samples were subjected to a twenty-hour drying period to eliminate moisture content. Subsequently, the samples were mounted on an aluminum stub, and a thin layer of gold (21 nm thickness) was sputter-coated onto the samples to make sample conductive. Micrographs were obtained using secondary electrons at a working distance of 9.5 mm.

Thermogravimetric Analysis (TGA):

We used the PerkinElmer TGA 4000 to do the TGA on the silica aerogel-nonwoven fabrics to find out what their TGA properties were. The samples weighed between 2 and 3 mg each. They were put in the sample pan and heated in a nitrogen atmosphere, with the temperature rising steadily from 50°C to 800°C at a rate of 10°C/min.

Attenuated Total Reflection Infrared (ATRIR) Spectroscopy:

Using a Thermo Scientific iS50 NIR Spectro-photometer with ATRIR spectroscopy, we looked at the chemical make-up of the silica aerogels.

A total of 128 scans were performed over a wave number range from 4000 cm^{-1} to 500 cm^{-1}, with a resolution of 4 cm^{-1}. The Analysis was conducted at room temperature.

2.2.3 Testing methods

To evaluate the heat-protective performance of the silica aerogel-embedded thermal liner, the samples were tested by a thermal protective performance (TPP) tester. Every specimen's heat transfer index (HTI24) was measured under radiative and flame exposure. According to ISO 6942 (2022) [25] and ISO 11613(2017) [26], the heat transfer index was the time

required to achieve a temperature rise of 24 °C in the calorimeter during the testing. The heat transfer index (HTI_{24}) ranks the ability of materials and material assemblies to restrict heat energy transfer through the test material. The testing instrument was developed according to ASTM F 1939 (2020) [27]. The samples were exposed to an incident heat flux in this device, and the backside temperature of the exposed fabric was recorded with a copper calorimeter. To produce radiant heat flux, a bank of five heating lamps was used, and the input voltage of the lamps was controlled by a variac to adjust the required heat flux. Two gas burners were used to generate flame heat flux, and the heat flux was controlled by controlling the gas flow. The temperature was measured by the copper calorimeter and sent to a computer via the ADAM processor, where the data was accumulated. Figure 1(c) depicts the instrument's schematic presentation, and Figure 1(d,e,f) represents the instrument under different working conditions. To adjust the required heat flux, at first, the temperature was measured without the test samples at a certain level of input voltage and gas flow rate. The heat flux was calculated using the equation below from the temperature data.

$$q = \frac{M.C_p.(Temp_{final} - Temp_{initial})}{absorptivity \;\; .A.(Time_{final} - Time_{initial})} \quad \ldots (1)$$

Where M denotes the mass of the copper calorimeter in kg, C_p is the specific heat of copper (J/kg K), and A is the calorimeter's surface area (m^2).

After that, with the trial-and-error method, the specific input voltage and the gas flow rate were selected for all the heat fluxes. ISO 9073-1:1989 [28] standard procedure was followed to determine the areal density of the samples. INSTRON 3365 instrument was utilized to measure the thickness of the samples in accordance with ISO 9073-2:1995 [29]. From the underneath equation, the bulk density of the specimens was calculated.

$$\text{Bulk density of fabric } (kg/m^3) = \frac{\text{Areal density of the fabric } (g/m^2)}{\text{Thickness of the fabric } (mm)} \quad \ldots (2)$$

The porosity of the samples was determined by employing the subsequent formula, which considers their bulk density:

$$\text{Porosity } (\%) = \left[1 - \frac{\text{Bulk density } \left(\frac{kg}{m^3}\right)}{\text{Fiber density } \left(\frac{kg}{m^3}\right)}\right] \times 100 \quad \ldots (3)$$

Paramount air permeability master was used to measure the air permeability of the specimen according to ISO 9073-15:2007 .[30]KES-F7-II Thermolabo tester was utilized to measure the thermal resistance of the samples in accordance with ISO 5085-1:1989 [31].

3 Results and discussions

3.1 Fabric morphology

The morphology of the needle-punched nonwoven fabric and the distribution of silica aerogel within the fabric were examined using scanning electron microscopy (SEM). Figure 2 illustrates the SEM images of silica aerogel-embedded nonwoven fabrics. Figures 2A, 2B, and 2C correspond to nonwoven samples with aerogel add-on percentages of 20 %, 40 %, and 60 %, respectively. Subfigures labeled (i), (ii), and (iii) represent samples with TMCS concentrations of 5 %, 10 %, and 15 %, respectively.

Based on the data, increasing the silica content results in a heavier coating of aerogel both on the fiber surfaces and within the nonwoven structure itself. We also see that the aerogel becomes noticeably more porous as the concentration of TMCS increases. This change is driven by the "spring-back" effect triggered by silylation. Essentially, as the gel dries at room temperature, the evaporation of internal liquids creates strong capillary forces that cause the material to shrink. However, the silylation treatment allows the structure to eventually "bounce back," preserving its porosity. To counteract this capillary force, surface modification of the gel structure is undertaken during the silylation stage. The re-expansion of the shrunken gel structure during silylation results in what is commonly known as the spring-back effect [32–34]. The spring-back effect is more prominent with higher amount of TMCS. Higher TMCS concentration causes a spring-back effect, increasing fabric thickness and porosity, as seen in SEM images. The increased porosity traps more air, which has very low thermal conductivity (about 0.026 $W \cdot m^{-1} \cdot K^{-1}$), thereby reducing heat transfer through the fabric. In addition, the more hydrophobic surface limits the heat transport. Overall, these changes lower heat transmission and improve the thermal insulation performance of the fabric.

3.2. Thermogravimetric Analysis

The thermal stability of the nonwoven fabric and the aerogel-embedded nonwoven fabrics with different add-on percentages was studied by a thermogravimetric analyzer under nitrogen purging. Figure 3(a) shows the thermograph of the nonwoven

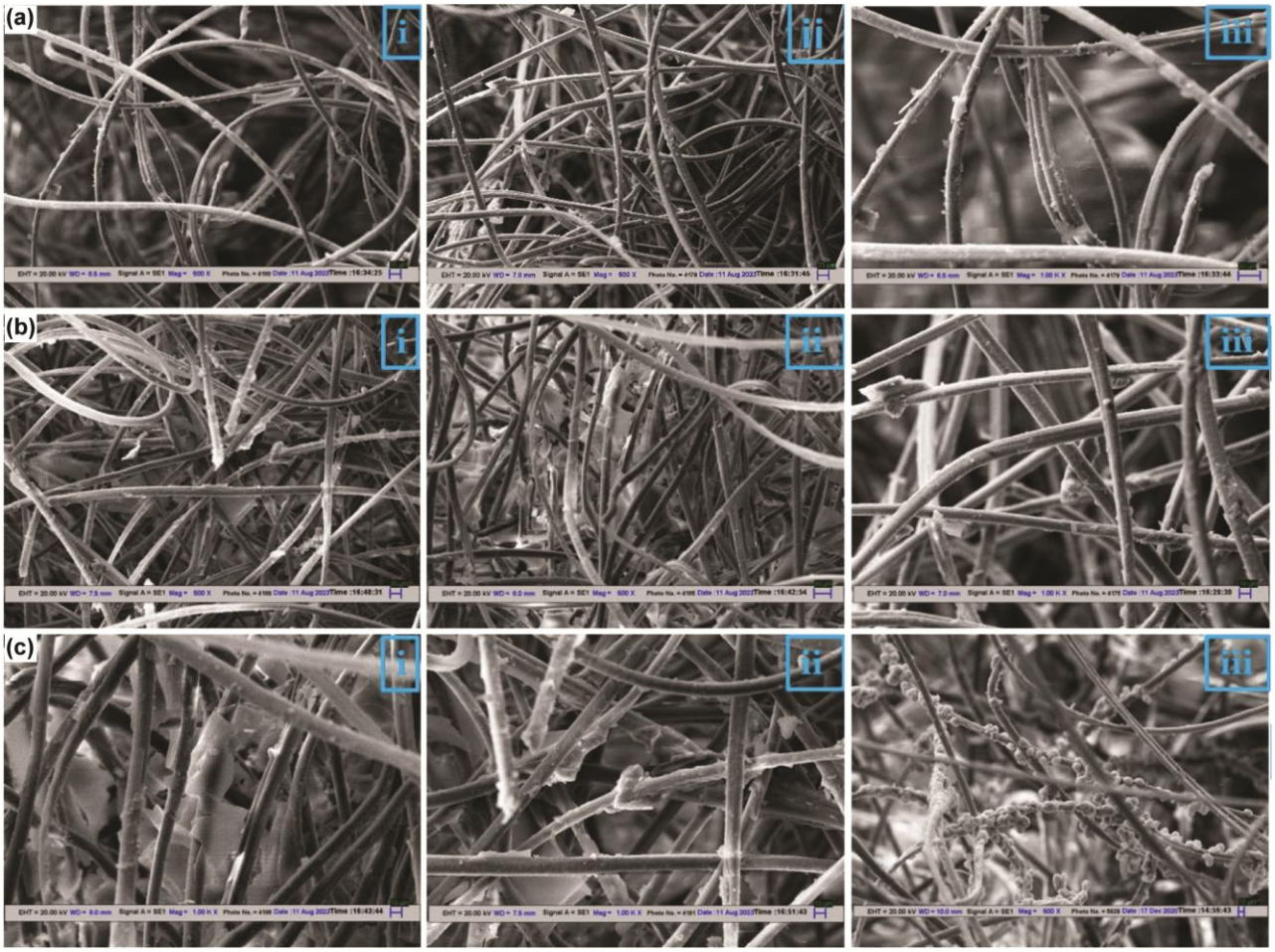

Figure 2 — (A) SEM image of aerogel embedded nonwoven fabric with add-on percentages of 20 %. (i) TMCS concentration 5 %, (ii) TMCS concentration 10 %, (iii) TMCS concentration 15 %; (B) — SEM image of aerogel embedded nonwoven fabric with add-on percentages of 40 %. (i) TMCS concentration 5 %, (ii) TMCS concentration 10 %, (iii) TMCS concentration 15 %; (C) — SEM image of aerogel-embedded nonwoven fabric with add-on percentages of 60 %. (i) TMCS concentration 5 %, (ii) TMCS concentration 10 %, (iii) TMCS concentration 15 %

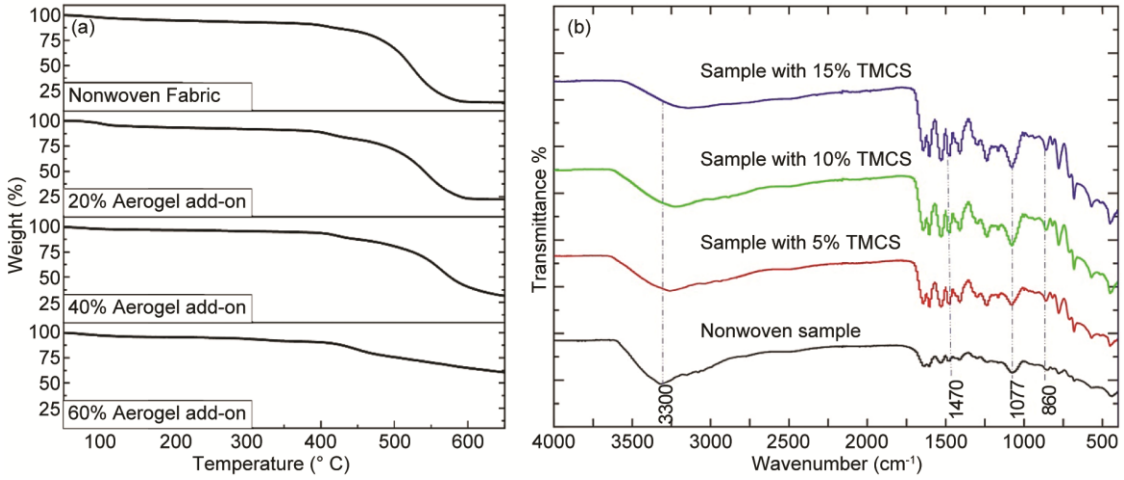

Figure 3 — (a) Thermograph of the nonwoven fabric and aerogel-embedded nonwoven fabric; (b) ATRIR spectra of test samples

fabric and aerogel-embedded nonwoven fabric with 20 %, 40 %, and 60 % add-on percentages.

In the thermograph of the nonwoven fabric, an initial weight loss is observed near 100°C, attributed to the evaporation of moisture within the sample. A sharp drop can be seen on the thermograph between 420°C and 500°C. This is the point at which the meta-aramid fibres start to break down thermally. When the temperature hits 650°C, the plain nonwoven fabric has lost most of its weight and only has 13% of its original weight left.

The samples with aerogel added to them break down in a similar way, but they are much more durable. The more silica aerogel there is, the better the material can handle very high temperatures. At 650°C, samples with 20%, 40%, and 60% aerogel "add-on" kept 22%, 33%, and 60% of their weight, respectively.

The results show that silica aerogel is much more stable at high temperatures than the fibre it is made of. In the end, the more aerogel you put into the fabric, the better it works when it's hot.

3.3. Attenuated total reflection infra-red (ATRIR) spectroscopy

Figure 3(b) shows the ATRIR spectra of both the nonwoven sample and the aerogel-embedded thermal liner, which had TMCS concentrations of 5%, 10%, and 15%. These spectra show what chemicals are in the test samples. The -OH group is represented by the wide peak that goes from 3200 cm^{-1} to 3600 cm^{-1}. The peak at 1470 cm^{-1} also shows that the C-H bonds in the CH_3 group are bending. A peak at 1077 cm^{-1} shows the Si-O-Si stretching, and a peak at 860 cm^{-1} shows the Si-C bond [32–34]. During silylation, the -OH groups that are already attached to silicon are replaced by the -O-Si–(CH_3)group from the silylating agent (TMCS) [35–37] . The broad peak between 3200 cm^{-1} and 3600 cm^{-1} gets less intense as the TMCS concentration goes up. This means that the concentration of -OH groups goes down. The peaks at 1077 cm^{-1} are stronger, which means that the Si-O-Si content goes up as the TMCS concentration goes up. The peak at 1470 cm^{-1} gets stronger as the concentration of TMCS rises, which suggests that more CH_3 groups are being added.

3.4. Physical Properties of Aerogel Embedded Liner:

Table 3 shows the thickness, air permeability, and thermal conductivity of the aerogel-enhanced thermal liner. This information gives a full picture of how the material works after being treated with aerogel. Figure 4(a) illustrates the relationship between thickness and add-on percentage, TMCS concentration. The black dot on the graph represents the thickness of the nonwoven thermal liner without aerogel treatment. From the graph, it is evident that the development of silica aerogel in situ within the nonwoven thermal

Table 3 — Physical properties of the aerogel embedded thermal liner

Sample no.	Add-on %	TMCS %	Thickness (mm)	Air Permeability ($cm^3/cm^2/s$)	Thermal conductivity (W/m-K)
1	20	5	7.44829	158.4	0.072376
2	20	10	7.61881	148.9	0.069129
3	20	15	7.7906	145.6	0.063452
4	40	5	7.3157	146.7	0.071087
5	40	10	7.51397	143.8	0.066509
6	40	15	7.75822	139.9	0.063906
7	60	5	6.94627	130.7	0.065441
8	60	10	7.22928	129.8	0.062982
9	60	15	7.7269	128.3	0.059586

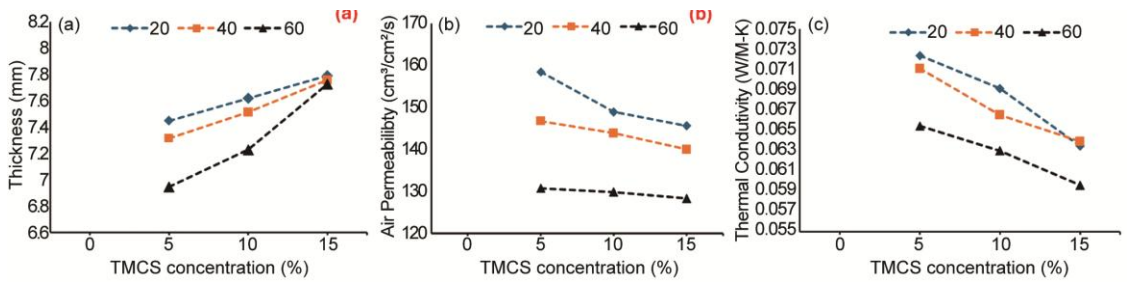

Figure 4 — (a) Relation between thickness and add-on percentage, TMCS concentration; (b) Relation between air permeability and add-on percentage, TMCS concentration; (c) Relation between thermal conductivity and add-on percentage, TMCS concentration

liner leads to a reduction in thickness values. The decrease in thickness is more pronounced with higher add-on percentages. This phenomenon could be attributed to the close vicinity during crosslinking between silica molecules, forming the aerogel in situ within the nonwoven structure. Moreover, the thickness value of the aerogel-embedded thermal liner increases with the rise in TMCS concentration for each level of add-on percentages. This increase may be attributed to the spring-back effect of silylation. Similar trends have been observed in the work of S. Poonam et al [38].

Figure 4 (b) illustrates the relationship between air permeability and add-on percentage, TMCS concentration. The black dot in the graph indicates the air permeability of the untreated thermal liner. The graph indicates that untreated thermal liner has highest air permeability, as the thickness and the porosity of the untreated thermal liner is higher. As the add-on percentage increases, the air permeability of the specimen decreases. This may happen due to the reduction of the thickness and the deposition of more amounts of silica in the nonwoven structure of the thermal liner. As the TMCS concentration increases due to spring-back effect, the aerogel structure's volume increases inside the nonwoven structure. Thus, this higher surface area of the aerogel restricts the air movement through the embedded thermal liner. Hence, the air permeability of the aerogel-embedded thermal liner decreases with the increase in TMCS concentration.

Figure 4(c) depicts the relationship between thermal conductivity and add-on percentage, as well as TMCS concentration. The black dot on the graph represents the thermal conductivity of the untreated nonwoven thermal liner. The TMCS-embedded liner shows a moderate reduction in air permeability (from 150 to 125 $cm^3/cm^2/s$) compared with typical commercial liners, due to increased thickness and pore filling by aerogel. The drop has affected thermal protection, but the numbers are still in an acceptable range because they provide a good balance of better thermal protection and good air flow. The untreated thermal liner also conducts heat energy better than the aerogel-infused thermal liner. Also, the thermal conductivity of the thermal liner goes down as the amount of silica aerogel goes up. This is because silica aerogel has very low thermal conductivity. With the increment of silica aerogel percentage, the thermal conductivity of the thermal liner diminishes due to the reduction in gas phase conduction, influenced by the meager pore size of the silica aerogel[39] and solid phase conduction facilitated by the aerogel matrix formed between fibrous contact points. A similar trend has been observed in the work of S. Shafi et al. [40]. Increase in TMCS concentration results in a decrease in the thermal conductivity of the thermal liner for every level of add-on percentage. This can be attributed to the higher thickness of the thermal liner with an increase in TMCS concentration induced by the spring-back effect. A comparable trend is noted in the study conducted by S. Chakraborty et al [37].

3.5. Heat protective performance:

Table 4 presents the Heat Transfer Index (HTI_{24}) values for both radiative and flame exposure for each test sample. Figure 5(a) shows the graph of the flame heat transfer index and the add-on percentage based on the concentration of TMCS. The black dot on the graph shows the HTI_{24} of the nonwoven thermal liner that hasn't been treated. The HTI_{24} of the thermal liners on the market shows that the one with silica aerogel has better thermal protection properties. When the percentages of add-on and TMCS concentrations are higher, the HTI_{24} of the radiative and flame HTI_{24} goes up from 35 seconds to 70 seconds and from 60 seconds to 110 seconds, respectively. It is also clear that the HTI_{24} value goes up as the add-on percentages go up for every concentration of TMCS. The more silica aerogel there is in the thermal liner, the less heat it can transfer. The HTI_{24} value goes up when the thermal conductivity of the aerogel embedded thermal liner goes down and the add-on percentages go up. It is observed that the HTI_{24} value increases with higher concentrations of TMCS for every concentration of add-on percentages. The reason is that when there is more TMCS, the thermal liner is thicker and has higher thermal conductivity.

HTI_{24} value increases with the rise in TMCS concentrations. This may be due to the lower thermal

Table 4 — Heat transfer index (HTI_{24}) value for radiative and flame exposure

Sample no.	Add-on %	TMCS %	Radiative HTI_{24}	Flame HTI_{24}
1	20	5	33	61
2	20	10	38	69
3	20	15	43	81
4	40	5	38	75
5	40	10	46	81
6	40	15	48	88
7	60	5	53	90
8	60	10	61	103
9	60	15	70	111

conductivity and higher thickness of the thermal liner with higher levels of TMCS concentrations.

Figure 5b shows how the Radiative Heat Transfer Index is connected to the add-on percentage (TMCS concentration). The black dot on the graph shows the HTI_{24} Thermal Liner that hasn't been treated. The graph shows that aerogel-embedded thermal liners are better at protecting against heat than the untreated nonwoven thermal liner, no matter how much TMCS is added or how high the percentage remains. For every level of TMCS concentrations, the HTI_{24} value of the aerogel embedded thermal liner increases with the increase in add-on percentage. This may occur due to the lower thermal conductivity and higher amount of silica deposited in situ thermal liner which restrict the heat flow through the test specimen and increases the thermal protective performance.

As the TMCS concentration increases the HTI_{24} value of the aerogel embedded thermal liner increases for every level of add-on percentage. This may occur due to the higher thickness of the thermal liner as TMCS concentration increases. Same kind of trend found in the flame exposure. But for the flame exposure the HTI_{24} value is higher than radiant exposure for every test sample. This may happen due to the higher penetration effect of the radiant heat exposure. The radiant heat can penetrate across the entire fabric width, which results in higher temperature rise rate at the back of the test samples, hence lower HTI_{24} value. The identical pattern may be found in the studies of B. Rajput et al. [41] and Y M Lee et al. [42].

3.6. Regression analysis:

Regression analysis has been carried out for both radiant and flame exposure to find out the impact of the independent parameters (add-on percentage, and TMCS concentration) on the dependent parameter (heat transfer index value). Table 5 represents the ANOVA table for radiant heat exposure. Lower significance F value (0.00045<0.05) and higher R^2 value (0.92) show the excellent correlation between the independent and dependent variables. The regression equation to predict the HTI_{24} value at different add-on percentages and different TMCS concentration under radiant heat exposure is listed as equation 4. Figure 6 (a) shows the experimental results under radiant heat exposure along with the prediction value obtained from the regression equation.

$$HTI_{24} = 12.11 + 0.583 \times Addon\ percentage + 1.2 \times TMCS\ concentration \quad \ldots (4)$$

Table 6 represents the ANOVA table for flame exposure. Lower significance F value ($3.71E^{-05}$<0.05) and higher R^2 value (0.96) show the excellent correlation between the independent and dependent variables. The regression equation to predict the HTI_{24} value at different add-on percentages and different TMCS concentrations under flame exposure is listed

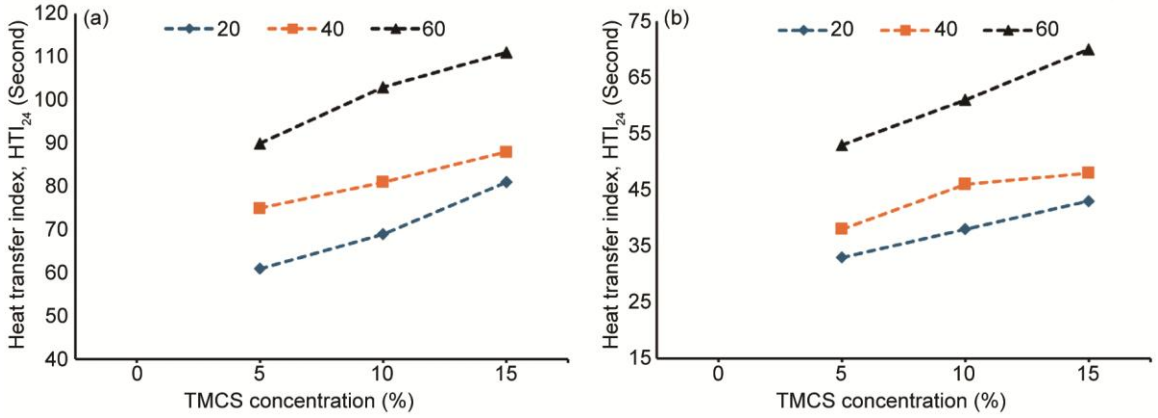

Figure 5 — (a) Relationship between flame heat transfer index and add-on percentage, TMCS concentration; (b) Relationship between radiative heat transfer index and add-on percentage, TMCS concentration

Table 5 — ANOVA table for radiant heat exposure

	df	*SS*	*MS*	*F*	*Significance F*
Regression	2	1044.833	522.4167	36.14413837	0.000450157
Residual	6	86.72222	14.4537		
Total	8	1131.556			

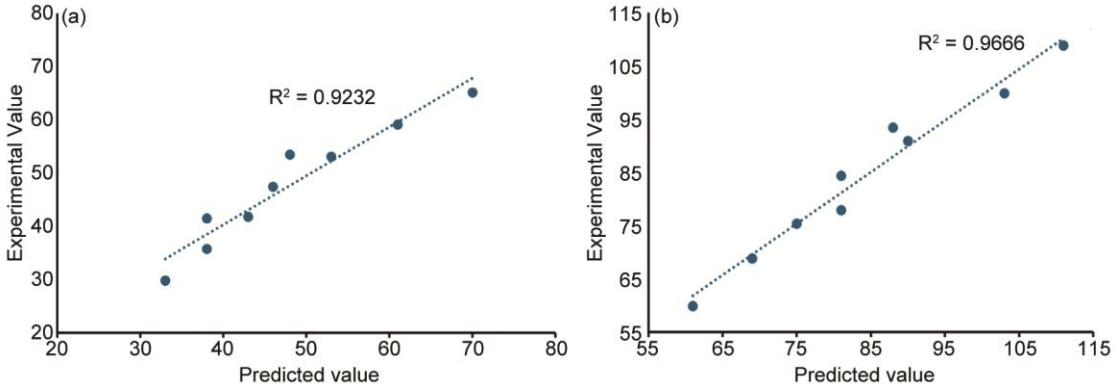

Figure. 6 — (a) Experimental and predicted values under radiant heat exposure; (b) Experimental and predicted values under flame heat exposure

Table 6 — ANOVA table for flame exposure

	df	*SS*	*MS*	*F*	*Significance F*
Regression	2	1927.5	963.75	86.95489	3.71E-05
Residual	6	66.5	11.08333		
Total	8	1994			

as equation 5. Figure 6 (b) shows the experimental results under flame exposure along with the prediction value obtained from the regression equation.

$$HTI_{24} = 35.33 + 0.775 \times Addon\ percentage + 1.8 \times TMCS\ concentration \quad \ldots (5)$$

4 Conclusion

TEOS based silica aerogel have been developed in situ nonwoven thermal liner using ambient pressure drying technique. The SEM image shows the increased porous structure of silica aerogel with the increase in silylating agent (trimethylchlorosilane (TMCS)) concentration. Thermogravimetric Analysis shows that the thermal stability of the aerogel embedded thermal liner increased with the rise in aerogel add-on percentages. The thermal conductivity of the aerogel embedded thermal liner decreases with the increase in both silica add-on percentages and the increased silylating agent (TMCS) concentration. Silica aerogel improves the thermal protective performance of the thermal liner. The HTI_{24} value of the aerogel embedded thermal liner is superior to untreated nonwoven thermal liner. The HTI_{24} value increases with higher add-on percentages and higher TMCS concentration. Regression study has been done for both radiative and flame heat exposure and from the study in can be seen good correlation between independent and dependent parameters for both radiative and flame exposure. The aerogel embedded thermal liners provide higher thermal protection in extreme conditions and can be used in multilayer fire fighter suits in the place of nonwoven thermal liner.

References

1 Fricke J. Aerogels — highly tenuous solids with fascinating properties. J Non Cryst Solids [Internet]. 1988;100(1): 169–73. Available from: https://www.sciencedirect.com/science/article/pii/0022309388900142

2 Fricke J, Emmerling A. Aerogels—Recent Progress in Production Techniques and Novel Applications. J Solgel Sci Technol [Internet]. 1998 Jan;13(1–3):299–303. Available from: https://link.springer.com/10.1023/A:1008663908431

3 Pierre AC, Pajonk GM. Chemistry of aerogels and their applications. Chem Rev [Internet]. 2002;102 11:4243–65. Available from: https://api.semanticscholar.org/CorpusID:29408316

4 Rafieian F, Dufresne A, Askari G, Rezaei A, Seyedhosseini-Ghaheh H, Jafari SM. Aerogels as novel ingredients: Production, properties and applications in medical, food and environmental sectors. Colloids Surf A Physicochem Eng Asp [Internet]. 2024 Apr;687:133410. Available from: https://linkinghub.elsevier.com/retrieve/pii/S0927775724002711

5 Schaefer DW, Keefer KD. Structure of Random Porous Materials: Silica Aerogel. Phys Rev Lett [Internet]. 1986 May 19;56(20):2199–202. Available from: https://link.aps.org/doi/10.1103/PhysRevLett.56.2199

6 Reisfeld R, JJørgensen CK, editors. Chemistry, Spectroscopy and Applications of Sol-Gel Glasses [Internet]. Berlin, Heidelberg: Springer Berlin Heidelberg; 1992. (Structure and Bonding; vol. 77). Available from: http://link.springer.com/10.1007/BFb0036963

7 Shewale PM, Rao AV, Rao AP. Effect of different trimethyl silylating agents on the hydrophobic and physical properties of silica aerogels. Appl Surf Sci [Internet]. 2008 Aug; 254(21):6902–7. Available from: https://linkinghub.elsevier.com/retrieve/pii/S0169433208009574

8 Prakash SS, Brinker CJ, Hurd AJ, Rao SM. Erratum: Silica aerogel films prepared at ambient pressure by using surface derivatization to induce reversible drying shrinkage. Nature [Internet]. 1995 Jun;375(6530):431–431. Available from: https://www.nature.com/articles/375431b0

9 Carlson G, Lewis D, McKinley K, Richardson J, Tillotson T. Aerogel commercialization: technology, markets and costs. J Non Cryst Solids [Internet]. 1995 Jun;186:372–9. Available from: https://linkinghub.elsevier.com/retrieve/pii/0022309395000690

10 Reisfeld Renata, Jorgensen CK. Chemistry, Spectroscopy and Applications of Sol-Gel Glasses / by Renata Reisfeld, Christian K. Jorgensen. Berlin, Heidelberg: Springer Berlin Heidelberg; 1992. (Structure and Bonding, 77).

11 Hrubesh LW. Aerogel applications. J Non Cryst Solids [Internet]. 1998 Apr;225:335–42. Available from: https://linkinghub.elsevier.com/retrieve/pii/S0022309398001355

12 Mulder CAM, van Lierop JG. Preparation, Densification and Characterization of Autoclave Dried SiO2 Gels. In 1986. p. 68–75. Available from: https://link.springer.com/10.1007/978-3-642-93313-4_8

13 Pajonk GM. Catalytic aerogels. Catal Today [Internet]. 1997 Mar;35(3):319–37. Available from: https://linkinghub.elsevier.com/retrieve/pii/S0920586196001630

14 Pajonk GM, Teichner SJ. On Some Recent Applications of Aerogels. In 1986. p. 193–9. Available from: https://link.springer.com/10.1007/978-3-642-93313-4_25

15 Gerlach R, Kraus O, Fricke J, Eccardt PCh, Kroemer N, Magori V. Modified SiO2 aerogels as acoustic impedance matching layers in ultrasonic devices. J Non Cryst Solids [Internet]. 1992;145:227–32. Available from: https://linkinghub.elsevier.com/retrieve/pii/S0022309305804612

16 Nasri W, Djebali R, Chamkha AJ, Bezazi A, Mechighel F, Reis P, et al. Thermal Behavior of Mesoporous Aramid Fiber Reinforced Silica Aerogel Composite for Thermal Insulation Applications: Microscale Modeling. Journal of Applied and Computational Mechanics [Internet]. 2024;10(1):140–51. Available from: https://jacm.scu.ac.ir/article_18499.html

17 Xue R, Liu G, Liu F. A simple and efficient method for the preparation of SiO2/PI/AF aerogel composite fabrics and their thermal insulation performance. Ceram Int [Internet]. 2023 Jan;49(1):210–5. Available from: https://linkinghub.elsevier.com/retrieve/pii/S027288422203139X

18 Katti A, Shimpi N, Roy S, Lu H, Fabrizio EF, Dass A, et al. Chemical, Physical, and Mechanical Characterization of Isocyanate Cross-linked Amine-Modified Silica Aerogels. Chemistry of Materials [Internet]. 2006 Jan 1;18(2):285–96. Available from: https://pubs.acs.org/doi/10.1021/cm0513841

19 Xue R, Chang Y, Liu F. Fabrication and performance evaluation of aramid laminated fabrics incorporated with silica composite aerogel for protective clothing. Ceram Int [Internet]. 2024 Apr;50(7):10348–54. Available from: https://linkinghub.elsevier.com/retrieve/pii/S0272884223042827

20 Baetens R, Jelle BP, Gustavsen A. Aerogel insulation for building applications: A state-of-the-art review. Energy Build [Internet]. 2011 Apr;43(4):761–9. Available from: https://linkinghub.elsevier.com/retrieve/pii/S0378778810004329

21 Lee KJ, Choe YJ, Kim YH, Lee JK, Hwang HJ. Fabrication of silica aerogel composite blankets from an aqueous silica aerogel slurry. Ceram Int [Internet]. 2018 Feb;44(2):2204–8. Available from: https://linkinghub.elsevier.com/retrieve/pii/S0272884217323829

22 Li Z, Gong L, Cheng X, He S, Li C, Zhang H. Flexible silica aerogel composites strengthened with aramid fibers and their thermal behavior. Mater Des [Internet]. 2016 Jun;99:349–55. Available from: https://linkinghub.elsevier.com/retrieve/pii/S0264127516303380

23 Li Z, Cheng X, He S, Shi X, Gong L, Zhang H. Aramid fibers reinforced silica aerogel composites with low thermal conductivity and improved mechanical performance. Compos Part A Appl Sci Manuf [Internet]. 2016 May;84:316–25. Available from: https://linkinghub.elsevier.com/retrieve/pii/S1359835X16000774

24 Das T, Das A, Alagirusamy R. Study on thermal protective performance of thermal liner in a multi-layer clothing under radiant heat exposure. Journal of Industrial Textiles [Internet]. 2022 Jun 21;51(5_suppl):8208S-8226S. Available from: https://journals.sagepub.com/doi/10.1177/15280837221094057

25 ISO. 6942:Protective clothing-Protection against heat and fire-Method of test: Evaluation of materials and material assemblies when exposed to a source of radiant heat. Switzerland. 2002.

26 ISO. 11613: Protective clothing for firefighter's who are engaged in support activities associated with structural fire fighting — Laboratory test methods and performance. 2017;2017.

27 ASTM. Test Method for Radiant Heat Resistance of Flame Resistant Clothing Materials with Continuous Heating [Internet]. West Conshohocken, PA: ASTM International; 2015. Available from: http://www.astm.org/cgi-bin/resolver.cgi?F1939-15

28 ISO. 9073-1 Textile - Test methods for nonwovens - Part 1. Vol. E. 19.

29 ISO. 9073-2 Textiles - Test methods for nonwovens - part 2. E. 1995.

30 ISO. 707:2008. ISO 9073-15 Textiles - Test methods for nonwovens - part 15. 61010-1 © Iec:2001. 2003;2003:13.

31 ISO. 5085-1 Textiles - Determination of thermal resistance-Part 1. 61010-1 © Iec:2001. 2003;2003:13.

32 Zemke F, Scoppola E, Simon U, Bekheet MF, Wagermaier W, Gurlo A. Springback effect of ambient-pressure-dried silica aerogels: nanoscopic effects of silylation revealed by in situ synchrotron X-ray scattering. Nanoscale Adv [Internet]. 2024;6(1):111–25. Available from: https://xlink.rsc.org/?DOI=D3NA00584D

33 Zemke F, Gonthier J, Scoppola E, Simon U, Bekheet MF, Wagermaier W, et al. Origin of the Springback Effect in Ambient-Pressure-Dried Silica Aerogels: The Effect of Surface Silylation. Gels [Internet]. 2023 Feb 16;9(2):160. Available from: https://www.mdpi.com/2310-2861/9/2/160

34 Zemke F, Scoppola E, Simon U, Bekheet MF, Wagermaier W, Gurlo A. Springback effect and structural features during the drying of silica aerogels tracked by in-situ synchrotron X-ray scattering. Sci Rep [Internet]. 2022 May 9;12(1):7537. Available from: https://www.nature.com/articles/s41598-022-11127-6

35 Johnson LM, Gao L, Shields IV CW, Smith M, Efimenko K, Cushing K, et al. Elastomeric microparticles for acoustic mediated bioseparations. J Nanobiotechnology

[Internet]. 2013 Dec 28;11(1):22. Available from: https://jnanobiotechnology.biomedcentral.com/articles/10.1186/1477-3155-11-22

36 Rao AP, Pajonk GM, Rao A V. Effect of preparation conditions on the physical and hydrophobic properties of two step processed ambient pressure dried silica aerogels. J Mater Sci [Internet]. 2005 Jul;40(13):3481–9. Available from: http://link.springer.com/10.1007/s10853-005-2853-3

37 Chakraborty S, Pisal AA, Kothari VK, Venkateswara Rao A. Synthesis and Characterization of Fibre Reinforced Silica Aerogel Blankets for Thermal Protection. Advances in Materials Science and Engineering [Internet]. 2016;2016: 1–8. Available from: http://www.hindawi.com/journals/amse/2016/2495623/

38 Shewale PM, Rao AV, Gurav JL, Rao AP. Synthesis and characterization of low density and hydrophobic silica aerogels dried at ambient pressure using sodium silicate precursor. Journal of Porous Materials [Internet]. 2009 Feb 11;16(1):101–8. Available from: http://link.springer.com/10.1007/s10934-007-9173-8

39 Lee SC, Cunnington GR. Conduction and Radiation Heat Transfer in High-Porosity Fiber Thermal Insulation. J Thermophys Heat Trans [Internet]. 2000 Apr;14(2):121–36. Available from: https://arc.aiaa.org/doi/10.2514/2.6508

40 Shafi S, Navik R, Ding X, Zhao Y. Improved heat insulation and mechanical properties of silica aerogel/glass fiber composite by impregnating silica gel. J Non Cryst Solids [Internet]. 2019 Jan;503–504:78–83. Available from: https://linkinghub.elsevier.com/retrieve/pii/S0022309318305568

41 Rajput B, Mahesh N, Rathour R, Das T, Ray B, Das A, et al. Performance analysis of multilayer flame-retardant fabric ensembles for different exposure conditions using numerical modeling. The Journal of The Textile Institute [Internet]. 2024 Feb 18;115(2):218–27. Available from: https://www.tandfonline.com/doi/full/10.1080/00405000.2022.2156717

42 Young Moo Lee, Barker RL. Effect of Moisture on the Thermal Protective Performance of Heat-Resistant Fabrics. J Fire Sci [Internet]. 1986 Sep 1;4(5):315–31. Available from: https://journals.sagepub.com/doi/10.1177/073490418600400502